

Iterative learning control in prosumer-based microgrids with hierarchical control[★]

Lia Streng^{*} Xiaohan Jing^{*} Ruth Boersma^{*} Paul Schultz^{**}
 Frank Hellmann^{**} Jürgen Kurths^{**} Jörg Raisch^{*}
 Thomas Seel^{*}

^{*} Technische Universität Berlin, Control Systems Group

{raisch,seel,streng}@control.tu-berlin.de

^{**} Potsdam Institute for Climate Impact Research

{hellmann,kurths,pschultz}@pik-potsdam.de

Abstract:

Power systems are subject to fundamental changes due to the increasing infeed of renewable energy sources. Taking the accompanying decentralization of power generation into account, the concept of prosumer-based microgrids gives the opportunity to rethink structuring and operation of power systems from scratch. In a prosumer-based microgrid, each power grid node can feed energy into the grid and draw energy from the grid. The concept allows for spatial aggregation such that also an interaction between microgrids can be represented as a prosumer-based microgrid. The contribution of this work is threefold: (i) we propose a decentralized hierarchical control approach in a network including different time scales, (ii) we use iterative learning control to compensate periodic demand patterns and save lower-layer control energy and (iii) we assure asymptotic stability and monotonic convergence in the iteration domain for the linearized dynamics and validate the performance by simulating the nonlinear dynamics.

Keywords: control of power systems, control of distributed systems, control of large-scale systems, networks, iterative learning control, convergence analysis, nonlinear systems

1. INTRODUCTION

Power systems are subject to fundamental changes due to the increasing infeed of renewable energy sources. Therefore adapted methods for modeling and simulation of power grids with respect to structuring and control are required. The concept of (prosumer-based) microgrids gives the opportunity to rethink structuring and operation of power systems from scratch (Schiffer et al., 2015). Microgrids refer to islanded or grid-connected areas with local balancing of production and demand. Like in classical power systems, in microgrids, hierarchical control is typically divided in primary, secondary and tertiary control, also called energy management, referring to the same tasks. Primary control is responsible for fast frequency stabilization and reacts in seconds, secondary control restores the frequency to its setpoint in terms of minutes and tertiary control refers to economic dispatch questions in the time scale of hours and days (Guerrero et al., 2010). In a prosumer-based microgrid, each grid node has local generation and load. With respect to hierarchical control including energy management, there is a variety of approaches summarized, e.g., in Bidram and Davoudi (2012), Dörfler et al. (2014), Olivares et al. (2014), Aamir et al. (2016), Xin et al. (2015), Han et al. (2016), Li

et al. (2017). While many contributions on hierarchical control for power systems review existing approaches for each control layer on the respective time scale, the aspect of explicitly studying their interaction has received little attention. In the present work, we consider different time scales from seconds to days. A strongly time-varying demand with a periodic baseline is assumed to be unknown and economic dispatch is not provided by higher-order market signals. Previous approaches for rejecting unknown periodic disturbances include adaptive internal model control, repetitive control and iterative learning control (ILC), see, e.g., Serrani et al. (2001); Roover et al. (2000); Bristow et al. (2006). Assuming that energy infeed planned ahead is available cheaper than instantaneous control power, we propose an ILC approach to address tertiary control with a notion of demand forecast. ILC is commonly applied to track a periodic reference signal or reject periodic disturbances. It reduces the error over the iteration cycles by adjusting a feedforward control input, and it can easily be combined with feedback controllers, cp. Jang et al. (1995); Doh (1999); Seel et al. (2013); Paszke et al. (2016). In power systems, ILC has mainly been applied for inverter control, e.g., Zeng et al. (2013); Teng (2014). Aamir et al. (2016) use ILC for an uninterruptible power supply and Chai et al. (2016) for optimal residential load scheduling. In building automation, Bampoulas et al. (2019) are using data-driven methods for demand response in the residential building sector and Yan et al.

[★] This work was funded by the Deutsche Forschungsgemeinschaft (DFG, German Research Foundation) – KU 837/39-1 / RA 516/13-1.

(2010) apply ILC to large-scale heating, ventilating and air-conditioning systems. In Guo et al. (2015), ILC is used for frequency control of power grids with high penetration of wind integration. In Guo et al. (2019), ILC is applied to energy management in electric vehicles. Most of the literature combining energy management and ILC focus on single nodes in a grid without an explicit overall power grid perspective. However, Nguyen and Banjerdpongchai (2016) review ILC for energy management in multi-agent systems and state that the applicability of ILC to the topic including physical constraints has a high research potential due to its (periodic) disturbance rejection capacity and distributed architecture for large-scale systems. With regards to networked control, there are several approaches using ILC in communication networks without physical coupling mainly focusing on data dropouts and communication delay, e.g., in Pan et al. (2006); Liu and Ruan (2016); Shen et al. (2017). In Xu and Yang (2013), ILC for physically interconnected linear large-scale systems is studied and applied to economic dispatch in power systems based on cost functions and constant demand assuming a strongly connected communication graph. In contrast, the present work investigates an approach that is based on power exchange between prosumers with a highly fluctuating demand and no a priori communication requirements.

Main contributions

- We propose a decentralized hierarchical control approach in a network including different time scales;
- we use an iterative learning control (ILC) to compensate periodic demand patterns and save lower-layer control energy;
- we assure asymptotic stability in the iteration domain for the linearized dynamics and validate the performance by simulating the nonlinear dynamics.

Notation $\text{diag}(D_1, \dots, D_n)$ denotes a diagonal matrix, whose diagonal entries are given by D_i for $i \in \{1, \dots, n\}$; \mathbf{A}^\top the transpose of a matrix \mathbf{A} ; δ_{jk} is the Kronecker delta; $\mathbf{1}_N$ denotes the identity matrix of size N and $\mathbf{0}_N$ a square matrix of size N , all of whose entries are 0. For a vector space V and a domain D , V^D is the set of all functions from D into V . $\|\cdot\|_2$ denotes the Euclidean norm. Vectors and matrices are printed in bold. A subindex of any quantity but t is indicating the node $j \in \mathcal{N} := \{1, \dots, N\}$, $N \in \mathbb{N}$.

2. MODELING

We use the common swing equation to model the voltage phase dynamics of the uncontrolled plant close to the synchronous operation point. While the model originates from the analysis of synchronous machines, in the prosumer scenario inertia may be provided by grid-forming inverters with access to some sort of fast-reacting storage. For the lower-layer control, we use a first-order system (sometimes also called "leaky integrator", Weitenberg et al. (2018)), to provide a decentralized frequency control. A higher-layer controller is designed to achieve further control objectives, such as CO₂ or cost reduction. We will assume that a high-level controller will set properties of the system at regular

intervals based on a sequence of measurements. At each node (or a subset of nodes) the high-level control will have different values which it can set for the following cycle. The generic system will be given in terms of the inputs u^{ILC} from the high-level controller with the disturbances P^d composed of periodic and fluctuating power demand components.

2.1 Nonlinear model with lower-layer control

We compose the overall system by node dynamics that are given by the well-known swing equation (Machowski et al., 2011; Schiffer et al., 2015). Hence, for each node $j \in \mathcal{N} := \{1, \dots, N\}$, we have

$$\dot{\phi}_j(t) = \omega_j(t), \quad (1a)$$

$$M_j \dot{\omega}_j(t) = u_j^{LI}(t) + u_j^{ILC}(t) - F_j(t) - P_j^d(t), \quad (1b)$$

$$F_j(t) = \sum_{k \in \mathcal{N}} K_{jk} \sin(\phi_j(t) - \phi_k(t)), \quad (1c)$$

where t is the time [s], ϕ_j [rad] is the voltage phase angle of node j in the co-rotating frame and $\omega_j := \dot{\phi}_j$ [rad/s] its instantaneous frequency deviation from the rated grid frequency. M_j [kgm²] denotes the (effective) inertia constant and F_j [W] the AC power flow between node j and all neighboring nodes. For the latter, $K_{jk} := V_j V_k Y_{jk}$ is the maximum power flow, given by the steady-state voltages V_j, V_k [V] as well as the nodal admittance of the transmission line $j-k$ with magnitude Y_{jk} [1/Ω] and phase $\pi/2$ [rad]. The network topology is encoded in the admittance matrix, hence $K_{jk} \neq 0$ when j and k are directly connected and $K_{jk} = 0$ otherwise, cp. Hellmann et al. (2018).

The input u_j^{ILC} [W] from the higher-layer controller as well as the input u_j^{LI} [W] from the lower-layer controller have the units of electric power. Furthermore, $P_j^d = P_j^f + P_j^p$ [W] is the uncontrolled net power demand at node j which accounts for the actual demand or uncontrollable infeed from renewable sources. It consists of a fluctuating part P_j^f and a periodic part P_j^p whose period is empirically known/estimated (see Appendix A). This period will be used to determine the update cycle of the higher-layer control.

To achieve the bounded frequency deviation in the lower layer, we use a robust decentralized first-order controller, Weitenberg et al. (2018), that we refer to as the *low-level controller*. The control law is given as:

$$u_j^{LI}(t) = -k_{P,j} \omega_j(t) + \chi_j(t), \quad (2a)$$

$$T_j \dot{\chi}_j(t) = -\omega_j(t) - k_{I,j} \chi_j(t), \quad (2b)$$

where χ_j [W] is the controller state variable; T_j [s], $k_{I,j}$ [(Ws)⁻¹] and $k_{P,j}$ [Ws] are constant parameters of the low-level controller. With this controller, bounded frequency deviation can be guaranteed by selecting the parameters accordingly, cp. (Weitenberg et al., 2018, Corollary 1). The plant under low-level control is referred to as the *compound plant* hereafter.

2.2 Linear approximation of the compound plant

The power flow between nodes in the network is quadratic in the complex voltage, hence the compound plant model is nonlinear. For our later analysis of the ILC, we linearize the compound plant model (Eq. (1)-(2)) using the *DC approximation* of small phase differences (e.g. Stott et al. (2009); Machowski et al. (2011)):

$$\sum_{k=1}^N K_{jk} \sin(\phi_j - \phi_k) \simeq \sum_{k=1}^N K_{jk} (\phi_j - \phi_k) = \sum_{k=1}^N \mathcal{L}_{jk} \phi_k, \quad (3)$$

where $\mathcal{L}_{jk} := \delta_{jk} \sum_{l=1}^N K_{jl} - K_{jk}$ is the entry jk of a weighted Laplacian matrix \mathcal{L} . The latter is symmetric and positive semidefinite, (Merris, 1994). We consider purely inductive lines here, but the approach is not limited to this assumption.

We obtain the following linear compound plant model:

$$\dot{\mathbf{x}}(t) = \mathbf{A}\mathbf{x}(t) + \mathbf{B}\mathbf{u}(t) + \mathbf{E}\mathbf{d}(t), \quad (4)$$

as a continuous-time ODE with a state vector $\mathbf{x} : \mathbb{R}_{\geq 0} \rightarrow \mathbb{R}^{3N}$, $\mathbf{x} = [\phi_1, \dots, \phi_N, \omega_1, \dots, \omega_N, \chi_1, \dots, \chi_N]^\top$, $\mathbf{u} = [u_1^{ILC}, \dots, u_N^{ILC}]^\top$ and $\mathbf{d} = [P_1^d, \dots, P_N^d]^\top$. We have $\mathbf{A} \in \mathbb{R}^{3N \times 3N}$ as follows

$$\mathbf{A} = \begin{bmatrix} \mathbf{0}_N & \mathbf{1}_N & \mathbf{0}_N \\ -\mathbf{M}^{-1}\mathcal{L} & -\mathbf{M}^{-1}\mathbf{K}_P & \mathbf{M}^{-1} \\ \mathbf{0}_N & -\mathbf{T}^{-1} & -\mathbf{T}^{-1}\mathbf{K}_I \end{bmatrix} \quad (5)$$

and

$$\mathbf{B} = \begin{bmatrix} \mathbf{0}_N \\ \mathbf{M}^{-1} \\ \mathbf{0}_N \end{bmatrix} \in \mathbb{R}^{3N \times N}, \quad \mathbf{E} = \begin{bmatrix} \mathbf{0}_N \\ -\mathbf{M}^{-1} \\ \mathbf{0}_N \end{bmatrix} \in \mathbb{R}^{3N \times N} \quad (6)$$

with $\mathbf{M} = \text{diag}(M_1, \dots, M_N)$, $\mathbf{K}_P = \text{diag}(k_{P,1}, \dots, k_{P,N})$, $\mathbf{T} = \text{diag}(T_1, \dots, T_N)$, $\mathbf{K}_I = \text{diag}(k_{I,1}, \dots, k_{I,N})$.

2.3 Lifted system representation

We want to design a higher-layer control for the model (4) which requires a specific system representation of the compound plant which relates the output to the input directly over the course of one cycle.

We partition the continuous time $t \in \mathbb{R}_{\geq 0}$ into cycles $I_c = [cT_d, (c+1)T_d)$, $c \in \mathbb{N}_0$, of length T_d . In our case we choose T_d to be one day due to the period of the disturbance. The input for the compound plant (4) is not arbitrary. Instead we can choose $\mathbf{u}(t)$ during the interval I_c only within some behavior $\mathcal{B}_{ILC} \subset (\mathbb{R}^N)^{I_c}$, which we assume to be the same for all daily intervals I_c . In our case we will choose hourly constant functions: We denote the duration of one hour as $\Delta = 60$ min. Then the start of the hour $h = 1, \dots, 24$ in cycle c is

$$t_h^c = cT_d + (h-1)\Delta. \quad (7)$$

Note that t is increasing from cycle to cycle and runs from 0 to ∞ . We can write the input as a sum over hours h and cycles c as

$$\mathbf{u}(t) = \sum_{h,c} \mathbf{u}^{c,h} b^h(t - cT_d) \in \mathbb{R}^N \quad (8)$$

where

$$b^h(t) = \begin{cases} 1 & \text{if } t \in [(h-1)\Delta, h\Delta), \\ 0 & \text{otherwise.} \end{cases} \quad (9)$$

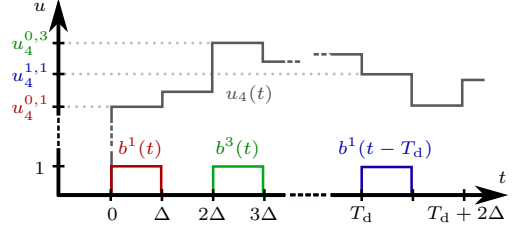


Fig. 1. Illustration of the composition of \mathbf{u} with the basis vectors $b^h(t)$, exemplary for $j = 4$

That is, $b^h(t)$ switches from 0 to 1 at the start of the hour, and back to 0 at the end. Hence, the hourly constant input then takes the values

$$\mathbf{u}(cT_d + h\Delta + \bar{\tau}) = \mathbf{u}^{c,h} \in \mathbb{R}^N, \quad (10)$$

for all $\bar{\tau} \in [0, \Delta)$. An illustration for the composition of \mathbf{u} is given in Figure 1. Corresponding to these inputs, we will record as output the node-wise control energy required by the lower layer per hour. Then, the hourly outputs are

$$\mathbf{y}^{c,h} = \int_{t_h^c}^{t_{h+1}^c} \mathbf{u}^{LI}(\tau) d\tau = \int_{t_h^c}^{t_{h+1}^c} \tilde{\mathbf{C}} \mathbf{x}(t) dt, \quad (11)$$

with

$$\tilde{\mathbf{C}} = [\mathbf{0}_N \quad -\mathbf{K}_P \quad \mathbf{1}_N]. \quad (12)$$

Related output approaches are investigated in Strenge et al. (2020). For stability over the cycles, we are interested in the behavior of the disturbance-free system and make use of the formal solution of (4). Within a cycle c we have:

$$\begin{aligned} \mathbf{y}^{c,h} &= \int_{t_h^c}^{t_{h+1}^c} \tilde{\mathbf{C}} \exp(\mathbf{A}(t - t_1^c)) \mathbf{x}(t_1^c) dt \\ &\quad + \int_{t_h^c}^{t_{h+1}^c} \int_{\tau=t_1^c}^t \tilde{\mathbf{C}} \exp(\mathbf{A}(t - \tau)) \mathbf{B} \mathbf{u}(\tau) d\tau dt \\ &= \mathbf{z}^{c,h} + \\ &\quad \sum_{h'=1}^{24} \int_{t_h^c}^{t_{h+1}^c} \int_{\tau=t_1^c}^t \tilde{\mathbf{C}} \exp(\mathbf{A}(t - \tau)) \mathbf{B} b^{h'}(\tau - t_1^c) d\tau dt \mathbf{u}^{c,h'}. \end{aligned} \quad (13)$$

In order to obtain the desired input-output relation over the course of one cycle, this suggests to introduce

$$\mathbf{P}^{c,hh'} = \int_{t_h^c}^{t_{h+1}^c} \int_{\tau=t_1^c}^t \tilde{\mathbf{C}} \exp(\mathbf{A}(t - \tau)) \mathbf{B} b^{h'}(\tau - t_1^c) d\tau dt. \quad (14)$$

Note that this is actually invariant under a shift of c , $\mathbf{P}^{c,hh'} = \mathbf{P}^{c+1,hh'}$ and we can drop the index c setting:

$$\mathbf{P}^{hh'} = \int_{t=(h-1)\Delta}^{h\Delta} \int_{\tau=0}^t \tilde{\mathbf{C}} \exp(\mathbf{A}(t - \tau)) \mathbf{B} b^{h'}(\tau) d\tau dt. \quad (15)$$

By Eq. (9), the $\mathbf{P}^{hh'}$ are causal in the hours, e.g., for $h' > h$ we get

$$\mathbf{P}^{hh'} = \mathbf{0}_N. \quad (16)$$

Again using Eq. (9) and shifting the integral bounds, the diagonal and off-diagonal are more explicitly given as

$$\mathbf{P}^{hh} = \int_{t=0}^{\Delta} \int_{\tau=0}^t \tilde{\mathbf{C}} \exp(\mathbf{A}(t-\tau)) \mathbf{B} d\tau dt, \quad (17)$$

and if $h > h'$, we have

$$\begin{aligned} \mathbf{P}^{hh'} &= \int_{t=0}^{\Delta} \int_{\tau=0}^{\Delta} \tilde{\mathbf{C}} \exp(\mathbf{A}((h-h')\Delta + t - \tau)) \mathbf{B} d\tau dt \\ &= \tilde{\mathbf{C}} \exp(\Delta \mathbf{A})^{h-h'} \int_{t=0}^{\Delta} \int_{\tau=0}^{\Delta} \exp(\mathbf{A}(t-\tau)) \mathbf{B} d\tau dt. \end{aligned} \quad (18)$$

In this way, we can write the input-output relationship for the disturbance-free system as

$$\mathbf{y}^{c,h} = \sum_{h'} \mathbf{P}^{hh'} \mathbf{u}^{c,h'} + \mathbf{z}^{c,h}. \quad (19)$$

By stacking the vectors and matrices $\mathbf{P}^{hh'}$,

$$\begin{aligned} \mathbf{y}^c &= \begin{bmatrix} \mathbf{y}_1^c \\ \mathbf{y}_2^c \\ \vdots \\ \mathbf{y}_{24}^c \end{bmatrix}, \quad \mathbf{u}^c = \begin{bmatrix} \mathbf{u}_1^c \\ \mathbf{u}_2^c \\ \vdots \\ \mathbf{u}_{24}^c \end{bmatrix}, \quad \mathbf{z}^c = \begin{bmatrix} \mathbf{z}_1^c \\ \mathbf{z}_2^c \\ \vdots \\ \mathbf{z}_{24}^c \end{bmatrix}, \\ \mathbf{P} &= \begin{bmatrix} \mathbf{P}^{11} & \mathbf{0}_N & \dots & \mathbf{0}_N \\ \vdots & \ddots & \ddots & \vdots \\ \vdots & & \ddots & \mathbf{0}_N \\ \mathbf{P}^{241} & \dots & \dots & \mathbf{P}^{2424} \end{bmatrix}, \end{aligned} \quad (20)$$

we can write (19) as

$$\mathbf{y}^c = \mathbf{P} \mathbf{u}^c + \mathbf{z}^c. \quad (21)$$

For the numerical implementation, we choose to further discretize the underlying continuous time and convert the integrals in the above relations to sums.

Note that choosing Δ much larger than the time constants of the compound plant would lead to time scale separation and to an approximately block diagonal \mathbf{P} . We present a general approach that avoids such assumptions and thus works also for much smaller segmentation intervals Δ .

3. CONTROLLER STRUCTURE AND DESIGN

Recall that the control consists of two layers, see Figure 2. The low-level controller (Eq. (2)) is responsible for bounded frequency deviation. High-level control acts on the compound plant described above, where the lower-layer control is already included. As specific high-level control, we choose an iterative learning control (ILC).

3.1 Control objectives

In order to understand the aim of the two-layer control approach, we make the following observation.

Observation 1. The day-ahead power is typically cheaper than the instantaneous control power.

Hence, the overall control objectives are the following:

- (1) Bounded frequency deviation:

$$\omega_j(t) \in [\omega_{\min}, \omega_{\max}] \quad \forall t \in \mathbb{R}_{\geq 0} \quad \text{and} \quad \forall j \in \mathcal{N}$$

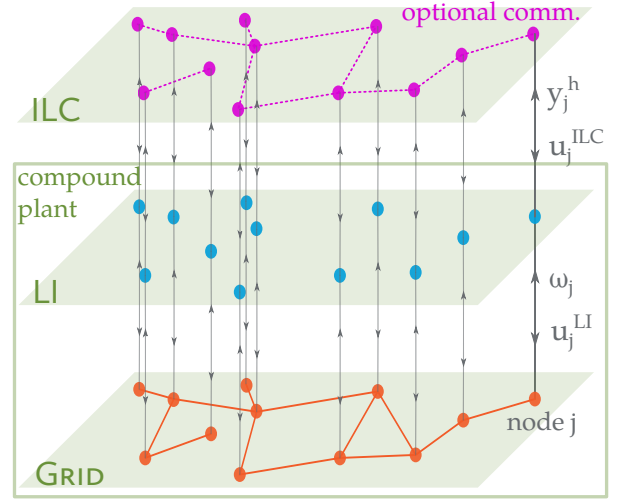


Fig. 2. Control architecture with low-level control (LI) and iterative learning controller (ILC)

- (2) Low-level control energy small:

$$\sum_{h=1}^{24} \|\mathbf{y}^{c,h}\|_2 = \sum_{h=1}^{24} \left\| \int_{t_h^c}^{t_{h+1}^c} \mathbf{u}^{LI}(\tau) d\tau \right\|_2 \ll \sum_{h=1}^{24} \|\mathbf{u}^{c,h}\|_2$$

for all $c \in \mathbb{N}_0$.

Note that (1) is achieved through the low-level control regardless of the additional higher-layer control input as long as $|\sum_{j \in \mathcal{N}} u_j^{ILC} - P_j^d| \leq |\sum_{j \in \mathcal{N}} P_j^d|$, (Weitenberg et al., 2018, Corollary 1). This is automatically satisfied for any sensible choice of ILC parameters.

3.2 Higher-layer control: iterative learning controller

The proposed ILC approach is applied to learn a power infeed that compensates the periodic demand component. We use an hourly update where each cycle c has a duration of one day, i.e. $h = 1 \dots 24$. A widely used learning law is implemented, which adjusts the daily input \mathbf{u}^c based on the low-level control energy \mathbf{y}^{c-1} of the previous cycle:

$$\mathbf{u}^c = \mathbf{Q}(\mathbf{u}^{c-1} - \mathbf{L} \mathbf{y}^{c-1}), \quad c > 0, \quad (22)$$

where $\mathbf{L} \in \mathbb{R}^{24N \times 24N}$ is the learning matrix, $\mathbf{Q} \in \mathbb{R}^{24N \times 24N}$ is called Q-filter, and the error from which the ILC learns is simply \mathbf{y}^{c-1} , since the desired low-level control energy is zero. We choose the initial input to be zero, i.e. $\forall h, j : u_j^{0,h} = 0$.

For \mathbf{Q} , we use a Butterworth low-pass filter with a relative cutoff frequency of $f_c = 1/6$. For \mathbf{L} we choose a diagonal matrix $\mathbf{L}(\kappa) = \kappa \mathbf{I}$ with a single scalar parameter $\kappa \in \mathbb{R}_{>0}$. Since only the first six Markov parameters of \mathbf{Q} are non-negligible, i.e., $Q_{ij}, 1 \leq i, j \leq 24, |j-i| \leq 6$, we can determine the ILC control input $\mathbf{u}^{c+1,h}$ of the next day 18 hours in advance.

The proposed ILC scheme has the capability to learn an *unknown* periodic demand, i.e., it reduces the required lower-layer control energy even if the periodic demand changes from known standard load curves to different periodic patterns (with daily period).

Identical initialization condition (i.i.c) In classical ILC, each cycle needs to start with the same initial condition. In this setting, we assume that the state \mathbf{x} returns to \mathbf{x}_0 at midnight when the demand is almost zero. This implies that $\mathbf{z}^c = \mathbf{z}^0 \forall c \in \mathbb{N}_0$. The reader is referred to the literature for relaxation of this condition, e.g., Jian-Xin (2005); Xu et al. (2006).

3.3 Learning dynamics

The ILC should be parametrized such that the following desirable convergence properties are achieved. Asymptotic stability here is referring to the input converging to a finite vector as c goes to infinity. Monotonic convergence means that in each cycle the error gets closer in some norm to the final error. We choose the 2-norm and hence require

$$\|\mathbf{e}^\infty - \mathbf{e}^{c+1}\|_2 \leq \gamma \|\mathbf{e}^\infty - \mathbf{e}^c\|_2, \quad (23)$$

where $0 \leq \gamma < 1$ and $\mathbf{e}^c = \mathbf{y}^{ref} - \mathbf{y}^c$ is the error in cycle c and \mathbf{e}^∞ denotes the asymptotic error $\lim_{c \rightarrow \infty} \mathbf{e}^c$. We use $\mathbf{e}^c = -\mathbf{y}^c$.

Theorem 1. (asymptotic stability in the iteration domain). (Bristow et al., 2006, p.101) The system (21),(22) is asymptotically stable for all \mathbf{u}^0 and \mathbf{z}^0 if and only if

$$\rho(\mathbf{Q}(\mathbf{I} - \mathbf{P}\mathbf{L})) < 1, \quad (24)$$

where $\rho(\cdot)$ denotes the spectral radius.

Theorem 2. (monotonic convergence). (Bristow et al., 2006, p.103) The system (21),(22) is monotonically convergent if

$$\bar{\sigma}(\mathbf{P}\mathbf{Q}\mathbf{P}^{-1}(\mathbf{I} - \mathbf{P}\mathbf{L})) < 1, \quad (25)$$

where $\bar{\sigma}(\cdot)$ denotes the maximum singular value. Then the left hand side of (25) is the convergence rate.

We consider a fully connected power grid of 4 nodes¹ with local high-level controllers, i.e., without additional communication. The model parameters are summarized in Table 1. With these parameters, the low-level controller has a bounded frequency deviation of 0.0038 Hz according to (Weitenberg et al., 2018, Corollary 1). The off-diagonal blocks of \mathbf{P} are in the order of 10% of the diagonal blocks, i.e., time scale separation would not be a good approximation.

Using these compound plant parameters, we determine the spectral radius and the maximum singular value as given in (24) and (25) for a large number of values of the learning gain $\kappa \in [0, 2] \text{ h}^{-1}$. The resulting design plot is presented in Figure 3. We can assure asymptotic stability in the iteration domain for $\kappa \in (0, 2] \text{ h}^{-1}$ and monotonic convergence of the error for $\kappa \in [0.025, 1.6775] \text{ h}^{-1}$. Furthermore, we predict that the fastest learning dynamics are achieved by a learning gain $\kappa = 1.205 \text{ h}^{-1}$ with a spectral radius of 0.205. For the sake of robustness, we choose a slightly smaller value, $\kappa = 1 \text{ h}^{-1}$, for which the spectral radius is clearly below 0.5.

4. PERFORMANCE EVALUATION

The proposed hierarchical controller, cp. Table 1, has been validated in extensive simulations of the overall nonlinear system model (1), (2), (22). Three main results are presented in the following. (i) We study initial convergence

¹ Note that scaling up is very straightforward.

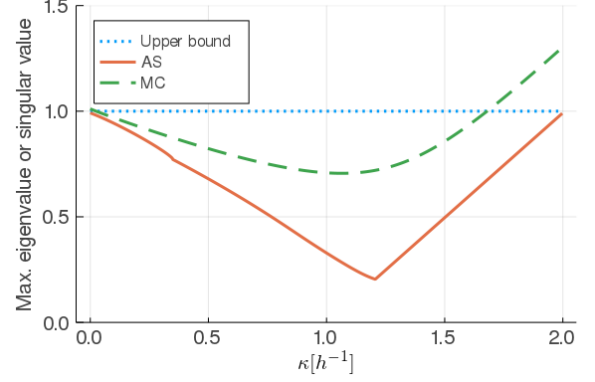


Fig. 3. Check for asymptotic stability (AS) in the iteration domain and monotonic convergence (MC) with different learning gains κ for $N = 4$ and 435 samples per hour

Table 1. Parameters (nodes $j, k = 1, \dots, N$)

Sym	Values	Unit	Description
κ_j	variable	1/h	learning parameter
\mathbf{K}_P	diag(400, 110, 100, 200)	Ws	parameter of lower-layer control
\mathbf{K}_I	diag(0.05, 0.004, 0.05, 0.001)	1/(Ws)	parameter of lower-layer control
K_{jk}	6	W/W	maximum power flow ($j \neq k$; j and k directly connected)
\mathbf{M}	diag(5, 4.8, 4.1, 4.8)	W s ²	inertia
N	4	-	number of nodes
\mathbf{T}	diag(0.04, 0.045, 0.047, 0.043)	1/W	parameter of lower-layer control

in a scenario with artificial step changes of the demand profile amplitude. (ii) We investigate the error dynamics in the iteration domain for different learning gains κ . (iii) We study a realistic learning scenario based on perturbed standard load profiles over several weeks.

Initial convergence Figure 4 (top) shows the sum over all nodes of the demand, the low-level control energy and the input from the ILC for a learning scenario with artificial step changes of the peak demand. The overall nonlinear model (1), (2), (22) of the closed-loop system is used, and the detailed synthetic demand model based on a squared sine curve with added noise is given in the Appendix A, Figure A.1 (left). The peak demand is stepping after three days and again after three or four more days (dotted light blue) and is different at each node (Figure 4, bottom). The (dashed) red line is the hourly integrated lower-layer control power $y_j^{c,h}$, and the solid black line shows u_j^{ILC} . It can be observed that the local ILC does not only learn the local demand. Instead, power sharing through the network is already achieved by the low-level controller during the first day. Hence, the ILC learns based on the synchronized state for the whole network reducing the lower-layer control energy at all nodes. The results of the summed quantities show that, after each demand peak step, the ILC learns to compensate the new demand and thereby decreases the low-level control energy to less than 10% of its original value within two days.

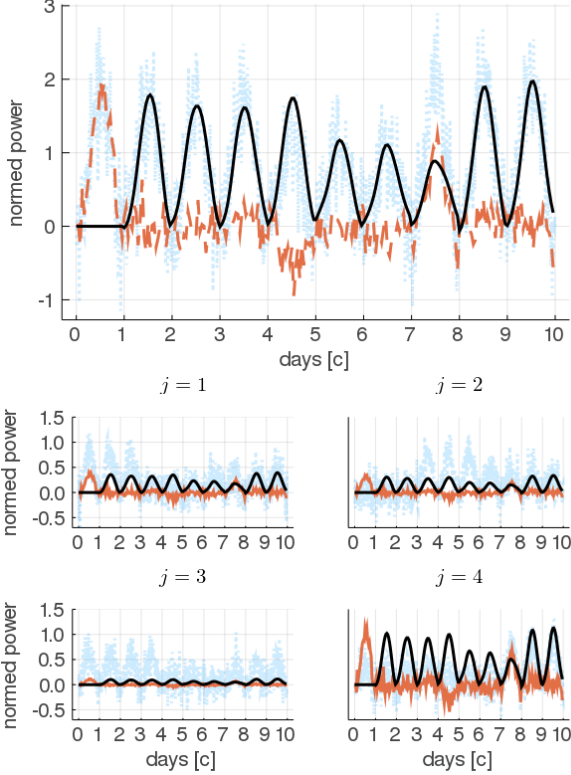


Fig. 4. Top: sum for all nodes $j = 1, 2, 3, 4$ and $\kappa = 1 \text{ h}^{-1}$; transparent blue: $\sum_j P_j^d$, dashed red: $\sum_j y_j^{c,h}$, solid black: $\sum_j u_j^{ILC}$; Bottom: separately for nodes $j = 1, 2, 3, 4$ and $\kappa = 1 \text{ h}^{-1}$; transparent blue: P_j^d , solid red: $y_j^{c,h}$, solid black: u_j^{ILC}

Error dynamics for different learning gains We study how the error convergence in the iteration domain depends on the choice of the scalar learning parameter κ . We use the nonlinear model as in the initial-convergence study with modified demand pattern. The periodic peak demand is between 0.6 and 0.9 W/W at the different nodes and fluctuating component varies randomly from day to day within $[0, 0.4]$ and $[0, 0.1]$ W/W, respectively. We consider a fine grid of different values of κ . For each value, we determine the error norm, i.e., a measure of the overall low-level control energy, for each of the first twenty days. Results are presented in Figure 5. The error norm is not converging for $\kappa = 2 \text{ h}^{-1}$ and it is constant for $\kappa = 0 \text{ h}^{-1}$ (no learning) over the cycles. The convergence of the error norm is fastest for $\kappa = 1 \text{ h}^{-1}$. These results agree with the above predictions, which are conservative statements based on the spectral radius and the maximum singular value of the linear model in Figure 3. The nonlinear dynamics are faster than predicted for this specific scenario.

Standard load curves To evaluate the performance of the proposed controller in more realistic scenarios, we employ standard load curves for selected consumer types in Germany, see Fünfgeld and Tiedemann (cited Oct 2019), with minute-wise added noise, cp. Figure A.1 (right). Note that the demand changes within one day and for the weekend. Simulating the overall nonlinear model of the

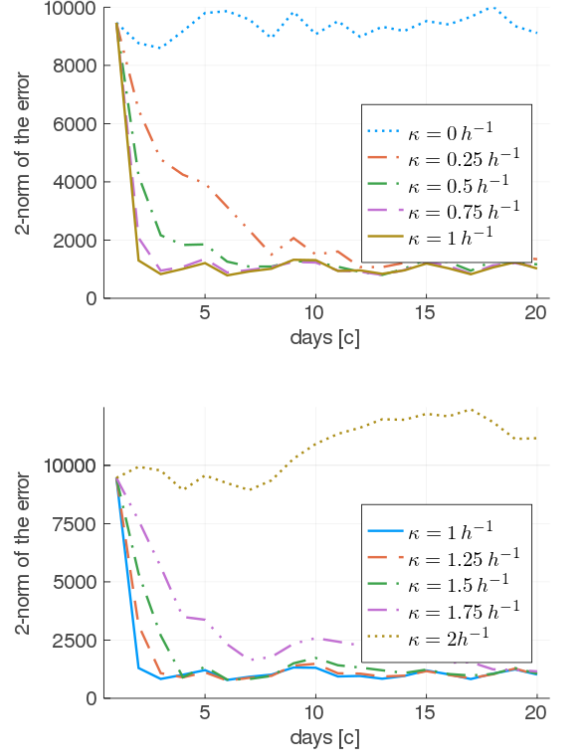


Fig. 5. Error norm ($\|e^c\|_2$) over the days for different learning gains with the nonlinear simulation

microgrid yields the results presented in Figure 6. The plot shows five weeks for the following three variables averaged over the hours for each cycle and summed over the nodes: the demand (dash-dotted green), the ILC control input (solid blue), the low-level control energy (dashed red). The proposed ILC achieves a sustainable reduction of the low-level control energy to less than 10% of the demand value. The weekly demand decrease that is associated with lower demands on weekends due to the productive use profiles leads to a rather mild periodic variation in \bar{y}^c . Note that this weekly demand variation, if deemed relevant, might be compensated by extending the proposed controller structure by another ILC with weekly periodicity.

5. CONCLUSIONS

We have presented a multi-timescale multilayer model of a prosumer-based microgrid and proposed a hierarchical control framework for it. Each node is controlled by a first-order controller on the lower layer and a local iterative learning control for the high-level controller. Our results of simulation studies of the overall nonlinear model show that the proposed controller quickly learns periodic portions of the daily demand variations even if they vary from day to day and therefore achieves the control objectives. Following the assumption that day-ahead power can be provided more efficiently and at lower costs than immediately available control energy, the proposed method has the potential for an advanced tertiary control in microgrids.

In future work, the dependency on other parameters like inertia and low-level control parameters should be

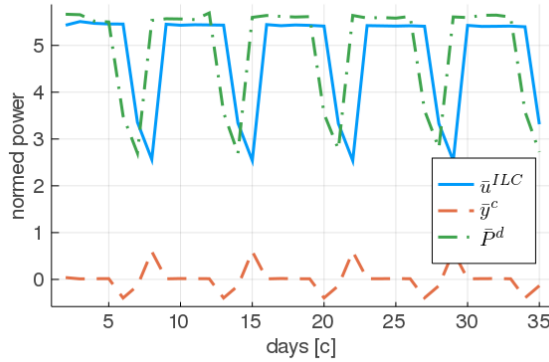


Fig. 6. Learning scenario over five weeks of work days and weekends (Saturday/Sunday) based on 1996 empirical household winter-term load profiles, $\kappa = 1 \text{ h}^{-1}$; the bar values are the sum over all nodes of the average over the hours in each cycle

studied. Different update intervals (other than hours) for the ILC may be considered and a comparison study with other tertiary control methods should be carried out. In particular, one may consider (i) methods using time scale separation and (ii) higher-order ILC or (iii) more classic low-level control such as an automatic generation control (AGC)-type implementation. Additional approaches for finding longer-term periodicity (week, season, year) can be applied or methods with varying cycle length, e.g., Li et al. (2015).

6. SOFTWARE

The code of the nonlinear model and linear matrices, eigenvalues and singular values is written in Julia 1.1.0 and is available on request or on the first author's github². The simulations were performed using the DifferentialEquations.jl package, Rackauckas and Nie (2017), and the Rodas4p solver, Wanner and Hairer (1996).

ACKNOWLEDGEMENTS

L.S. thanks Chris Macnab and Philipp Schulze for the constructive discussions and Jan Meyer-Dulheuer for helping to focus.

REFERENCES

- Aamir, M., Kalwar, K.A., and Mekhilef, S. (2016). Uninterruptible power supply (UPS) system. *Renewable and sustainable energy reviews*, 58, 1395–1410.
- Bampoulas, A., Saffari, M., Pallonetto, F., Mangina, E., and Finn, D.P. (2019). Self-learning control algorithms for energy systems integration in the residential building sector. In *2019 IEEE 5th World Forum on Internet of Things (WF-IoT)*, 815–818. IEEE.
- Bidram, A. and Davoudi, A. (2012). Hierarchical structure of microgrids control system. *IEEE Transactions on Smart Grid*, 3(4), 1963–1976.
- Bristow, D.A., Tharayil, M., and Alleyne, A.G. (2006). A survey of iterative learning control. *IEEE control systems magazine*, 26(3), 96–114.

- Chai, B., Yang, Z., Gao, K., and Zhao, T. (2016). Iterative learning for optimal residential load scheduling in smart grid. *Ad Hoc Networks*, 41, 99–111.
- Doh, T.Y. (1999). Robust iterative learning control with current feedback for uncertain linear systems. *International Journal of Systems Science*, 30(1), 39–47.
- Dörfler, F., Simpson-Porco, J.W., and Bullo, F. (2014). Plug-and-play control and optimization in microgrids. In *53rd IEEE Conference on Decision and Control*, 211–216. IEEE.
- Fünfgeld, C. and Tiedemann, R. (cited Oct 2019). Bundesverband der Energie- und Wasserwirtschaft Website. www.bdew.de/energie/standardlastprofile-strom.
- Guerrero, J.M., Vasquez, J.C., Matas, J., De Vicuña, L.G., and Castilla, M. (2010). Hierarchical control of droop-controlled AC and DC microgrids - A general approach toward standardization. *IEEE Transactions on industrial electronics*, 58(1), 158–172.
- Guo, H.q., Liu, C.z., Yong, J.w., Cheng, X.q., and Muhammad, F. (2019). Model predictive iterative learning control for energy management of plug-in hybrid electric vehicle. *IEEE Access*.
- Guo, W., Liu, F., Si, J., He, D., Harley, R., and Mei, S. (2015). Online supplementary ADP learning controller design and application to power system frequency control with large-scale wind energy integration. *IEEE transactions on neural networks and learning systems*, 27(8), 1748–1761.
- Han, Y., Li, H., Shen, P., Coelho, E.A.A., and Guerrero, J.M. (2016). Review of active and reactive power sharing strategies in hierarchical controlled microgrids. *IEEE Transactions on Power Electronics*, 32(3), 2427–2451.
- Hellmann, F., Schultz, P., Jaros, P., Levchenko, R., Kapitaniak, T., Kurths, J., and Maistrenko, Y. (2018). Network-induced multistability: Lossy coupling and exotic solitary states. *arXiv preprint arXiv:1811.11518*.
- Jang, T.J., Choi, C.H., and Ahn, H.S. (1995). Iterative learning control in feedback systems. *Automatica*, 31(2), 243–248.
- Jian-Xin, X. (2005). Recent advances in iterative learning control. *自动化学报*, 31(1), 132–142.
- Li, X., Xu, J.X., and Huang, D. (2015). Iterative learning control for nonlinear dynamic systems with randomly varying trial lengths. *International Journal of Adaptive Control and Signal Processing*, 29(11), 1341–1353.
- Li, Z., Zang, C., Zeng, P., Yu, H., and Li, S. (2017). Fully distributed hierarchical control of parallel grid-supporting inverters in islanded AC microgrids. *IEEE Transactions on Industrial Informatics*, 14(2), 679–690.
- Liu, J. and Ruan, X. (2016). Networked iterative learning control approach for nonlinear systems with random communication delay. *International Journal of Systems Science*, 47(16), 3960–3969.
- Machowski, J., Bialek, J., and Bumby, J. (2011). *Power system dynamics: Stability and control*. John Wiley & Sons, Ltd.
- Merris, R. (1994). Laplacian matrices of graphs: A survey. *Linear algebra and its applications*, 197, 143–176.
- Nguyen, D.H. and Banjerdpongchai, D. (2016). Iterative learning control of energy management system: Survey on multi-agent system framework. *Engineering Journal*, 20(5), 1–4.

² <https://github.com/strangeli/>

Olivares, D.E., Mehrizi-Sani, A., Etemadi, A.H., Cañizares, C.A., Iravani, R., Kazerani, M., Hajimiragha, A.H., Gomis-Bellmunt, O., Saeedifard, M., Palma-Behnke, R., et al. (2014). Trends in microgrid control. *IEEE Transactions on smart grid*, 5(4), 1905–1919.

Pan, Y.J., Marquez, H.J., and Chen, T. (2006). Sampled-data iterative learning control for a class of nonlinear networked control systems. In *2006 American Control Conference*, 6–pp. IEEE.

Paszke, W., Rogers, E., and Galkowski, K. (2016). Experimentally verified generalized KYP lemma based iterative learning control design. *Control Engineering Practice*, 53, 57–67.

Rackauckas, C. and Nie, Q. (2017). Differentialequations.jl—a performant and feature-rich ecosystem for solving differential equations in julia. *Journal of Open Research Software*, 5(1).

Roover, D.D., Bosgra, O.H., and Steinbuch, M. (2000). Internal-model-based design of repetitive and iterative learning controllers for linear multivariable systems. *International Journal of Control*, 73(10), 914–929.

Schiffer, J., Zonetti, D., Ortega, R., Stankovic, A., Sezi, T., and Raisch, J. (2015). Modeling of microgrids - from fundamental physics to phasors and voltage sources. *Automatica*, 1–15.

Seel, T., Weber, S., Affeld, K., and Schauer, T. (2013). Iterative learning cascade control of continuous noninvasive blood pressure measurement. In *IEEE International Conference on Systems, Man, and Cybernetics*, 2207–2212. Manchester, UK.

Serrani, A., Isidori, A., and Marconi, L. (2001). Semi-global nonlinear output regulation with adaptive internal model. *IEEE Transactions on Automatic Control*, 46(8), 1178–1194.

Shen, D., Zhang, C., and Xu, Y. (2017). Two updating schemes of iterative learning control for networked control systems with random data dropouts. *Information Sciences*, 381, 352–370.

Stott, B., Jardim, J., and Alsac, O. (2009). DC Power Flow Revisited. *IEEE Transactions on Power Systems*, 24(3), 1290–1300.

Streng, L., Schultz, P., Kurths, J., Raisch, J., and Hellmann, F. (2020). A multiplex, multi-timescale model approach for economic and frequency control in power grids. *Chaos: An Interdisciplinary Journal of Nonlinear Science*, 30(3), 033138.

Teng, K.T. (2014). *Repetitive and iterative learning control for power converter and precision motion control*. Ph.D. thesis, UCLA.

Wanner, G. and Hairer, E. (1996). *Solving ordinary differential equations II*. Springer Berlin Heidelberg.

Weitenberg, E., Jiang, Y., Zhao, C., Mallada, E., Dörfler, F., and De Persis, C. (2018). Robust decentralized frequency control: A leaky integrator approach. In *2018 European Control Conference (ECC)*, 764–769.

Xin, H., Zhao, R., Zhang, L., Wang, Z., Wong, K.P., and Wei, W. (2015). A decentralized hierarchical control structure and self-optimizing control strategy for FP type DGs in islanded microgrids. *IEEE Transactions on Smart Grid*, 7(1), 3–5.

Xu, J.X., Yan, R., and Chen, Y. (2006). On initial conditions in iterative learning control. In *2006 American Control Conference*, 6–pp. IEEE.

Xu, J.X. and Yang, S. (2013). Iterative learning based control and optimization for large scale systems. *IFAC Proceedings Volumes*, 46(13), 74–81.

Yan, X., Ren, Q., and Meng, Q. (2010). Iterative learning control in large scale HVAC system. In *2010 8th World Congress on Intelligent Control and Automation*, 5063–5066. IEEE.

Zeng, Z., Yang, H., Zhao, R., and Cheng, C. (2013). Topologies and control strategies of multi-functional grid-connected inverters for power quality enhancement: A comprehensive review. *Renewable and Sustainable Energy Reviews*, 24, 223–270.

Appendix A. DEMAND MODEL

A.1 Synthetic demand model

As a benchmark for the proposed ILC control, we consider synthetic demand curves. For every node $j \in \mathcal{N}$ in the network, the demand P_j^d is dominated by a periodic baseline P_j^p (see Fig. A.1, left):

$$P_j^p(t) = H_j \sin^2\left(\pi \frac{t}{T_d}\right),$$

where the period T_d [s] is the duration of a day and the demand amplitudes $H_j \sim \mathcal{U}([0; 1])$ [W/W] are uniform i.i.d. random numbers. At the beginning t_h^c of each hour h in cycle c , the nodal demands are updated as

$$P_j^d(t_h^c) = P_j^p(t_h^c) + G_j \eta_{j,h} \quad (\text{A.1})$$

subject to random fluctuations. The fluctuation amplitudes G_j are set to 0.2 W/W. $\eta_{j,h}$ is an uncorrelated Gaussian process with zero mean and unit variance, i.e. $\langle \eta_{j,h} \eta_{j',h'} \rangle = \delta_{j,j'} \delta_{h,h'}$. The demand P_j^d is linearly interpolated over the interval $[t_h^c; t_{h+1}^c]$ between two consecutive updates.

A.2 Standard load profiles

We use H0 (node 1), G1 (node 2) and G4 (node 3) standard load profiles and a mixed profile of these three (node 4) which are representing households (H0) and productive use (G1, G4) in a winter week, cp. Fünfgeld and Tiedemann (cited Oct 2019). They are normed with 100 W and distinguish between week days, Saturday and Sunday. We add minute-wise random noise of up to 10% to each node. An exemplary week of a H0 profile can be seen in Figure A.1 (right).

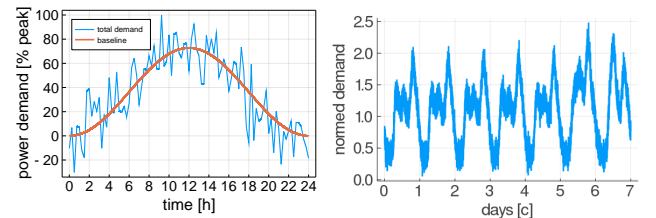


Fig. A.1. Exemplary synthetic demand curve for one day (left); exemplary demand curve based on the H0 standard load profile for one week (right)